Face Centered Cubic and Hexagonal Close Packed Skyrmion Crystals in Centrosymmetric Magnets

Shi-Zeng Lin and Cristian D. Batista

Face centered cubic and hexagonal close packed skyrmion crystals in centro-symmetric magnets

Shi-Zeng Lin[1, *] and Cristian D. Batista[2, 3]

[1]*Theoretical Division, T-4 and CNLS, Los Alamos National Laboratory, Los Alamos, New Mexico 87545, USA*
[2]*Department of Physics and Astronomy, The University of Tennessee, Knoxville, Tennessee 9 37996, USA*
[3]*Quantum Condensed Matter Division and Shull-Wollan Center,*
Oak Ridge National Laboratory, Oak Ridge, Tennessee 37831, USA
(Dated: January 17, 2018)

Skyrmions are disk-like objects that typically form triangular crystals in two dimensional systems. This situation is analogous to the so-called "pancake vortices" of quasi-two dimensional superconductors. The way in which skyrmion disks or *pancake skyrmions* pile up in layered centro-symmetric materials is dictated by the inter-layer exchange. Unbiased Monte Carlo simulations and simple stabilization arguments reveal face centered cubic and hexagonal close packed skyrmion crystals for different choices of the inter-layer exchange, in addition to the conventional triangular crystal of skyrmion lines. Moreover, an inhomogeneous current induces sliding motion of pancake skyrmions, indicating that they behave as effective mesoscale particles.

Magnetic skyrmions are swirling spin textures, which have been recently discovered in magnets without inversion symmetry [1, 2]. Protected by their nontrivial topology, skyrmions are robust against small perturbations and can be driven by various external stimuli [3–12]. Because of their compact size, their high mobility and the possibility of creating or destroying them with electric currents, skyrmions are regarded as promising candidates for applications in memory devices [13–16]. It is known by now that skyrmions are rather ubiquitous topological magnetic strcutures because they have been observed in several classes of magnetic materials *without inversion symmetry*, including metals [1, 2], semiconductors [17], insulators and multiferroics [18, 19]. In bulk, skyrmion structures typically appear as triangular crystals of straight lines parallel to H. This phenomenon is analogous to the Abrikosov vortex lattice of type II superconductors. However, the skyrmion crystal (SC) phase of non-centrosymmetric magnets is only a small pocket of the thermodynamic phase diagram. In thin films, skyrmions become pancake-like objects that still form a triangular lattice. In contrast to the 3D case, this phase is stable over a wide field and temperature region extending down to $T = 0$.

Different non-centrosymmetric or chiral magnets exhibit similar skyrmion phase diagrams because the linear skyrmion size, l_s, is much bigger than the atomic lattice parameter: $l_s/a >> 1$. This dimensionless ratio is of the order of J/D, where J is the ferromagnetic exchange constant and D is the magnitude of a Dzyaloshinskii-Moriya (DM) interaction [20–22] arising from the lack of inversion symmetry. The phase diagram is satisfactorily described by an effective continuum model including ferromagnetic exchange, the DM interaction and the Zeeman term [23–25].

Given that most materials have inversion symmetry, it is relevant to ask if skyrmion crystals can emerge in centro-symmetric magnets. According to Derrick's theorem [26], stable topological excitations require the existence of a characteristic length scale. Competing interactions in frustrated magnets can provide this length scale. [27] For instance, helical magnetic orderings,which are quite ubiquitous in rare-earth magnets [28], have a characteristic length $2\pi/|Q|$ asso-

ciated to their propagation vector Q. Indeed, localized spin textures can be stabilized by competing interactions. [29–31] Centro-symmetric magnets support skyrmions with any sign of the of scalar spin chirality (the skyrmion charge can be positive or negative). Moreover, skyrmions of uniaxial magnets can have arbitrary *helicity* [14], because of the $U(1)$ symmetry of spin rotation along the field-axis. Besides the additional Goldstone mode of this internal degree of freedom, skyrmions in centro-symmetric magnets have interesting properties not shared by skyrmions of chiral magnets [32–38].

The triangular skyrmion lattice can be regarded as a superposition of three single-Q magnetic helices with propagation vectors differing by $\pm120°$ rotations. The triple-Q superposition forces a spatial modulation of the *magnitude* of the magnetic moment, which has an exchange energy cost. In uniaxial 2D magnets with easy-axis anisotropy, this energy cost can be compensated by an anisotropy energy gain [32, 39]. Indeed, skyrmions have been recently observed in the centro-symmetric materials [28, 40]. However, it is unclear how these pancake skyrmions organize in 3D layered magnets. In this Letter, we study 3D skyrmion crystals emerging in frustrated Heisenberg models on a vertically stacked triangular lattice. We demonstrate that frustration of the inter-layer exchange leads to multiple ways of stacking pancake skyrmions along the c-axis. Small $Q_z \ll 1$ values lead to triangular SC's of tilted lines relative to the external magnetic field. In contrast, larger values of Q_z produce hexagonal close packed (HCP) and face centered cubic (FCC) crystals of pancake skyrmions.

We consider the spin Hamiltonian

$$\mathcal{H} = \sum_{i \neq j} J_{ij}S_i \cdot S_j - H \sum_i S_{i,z} - A \sum_i S_{i,z}^2, \qquad (1)$$

defined on a vertically stacked triangular lattice, which includes an easy-axis anisotropy term ($A > 0$). The external magnetic field H is assumed to be parallel to the c-axis. The intra-layer exchange includes a nearest-neighbor (NN) ferromagnetic (FM) coupling, $J_1 < 0$, and a third NN antiferromagnetic (AFM) interaction $J_3 > 0$. The inter-layer exchange is also assumed to be frustrated. We fix the ratio $J_3/J_1 = -0.5$,
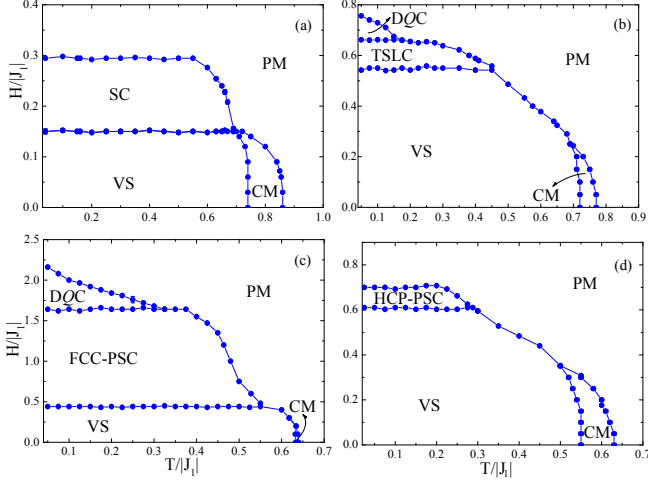
FIG. 1. (color online) Temperature-magnetic field phase diagram for the Hamiltonian of Eq. (1) with (a) $Q_z = 0$, (b) $Q_z = 2\pi/5$, (c) $Q_z = 2\pi/3$ and (d) $Q_z = \pi$, obtained from Monte Carlo simulations. The easy-axis anisotropy is $A = 0.5|J_1|$. In (a) the interlayer exchange is $J_1^c = 0.5J_1$ between adjacent layers and $J_2^c = 0$ between NNN layers. In (b), $J_1^c = 0.5J_1$ and $J_2^c = -0.4045J_1^c$. In (c), $J_1^c = -0.5J_1$ and $J_2^c = -0.25J_1$. In (d), $J_1^c = -0.2J_1$ and $J_2^c = 0$.

corresponding to a magnitude of the ordering wave vector $Q_{ab} = 2\cos^{-1}[(1 + \sqrt{1 - 2J_1/J_3})/4] = 2\pi/5$ [41]. The 2D limit of this Hamiltonian includes a triangular SC in its phase diagram. [32, 39]

The exchange interaction in momentum space is

$$\mathcal{H}_{\text{ex}} = \sum_{i \neq j} J_{ij} \mathbf{S}_i \cdot \mathbf{S}_j = \sum_{\mathbf{q}} J(\mathbf{q}) \mathbf{S}(\mathbf{q}) \cdot \mathbf{S}(-\mathbf{q}), \quad (2)$$

where $J(\mathbf{q})$ and $S(\mathbf{q})$ are the Fourier transform of J_{ij} and $\mathbf{S}_i$. The ground state is a helix with an ordering wave vector $\mathbf{Q}$ that minimizes $J(\mathbf{q})$. The easy-axis anisotropy distorts the helix by inducing higher harmonics that increase the easy-axis spin component. If $J(\mathbf{q})$ is minimized by six ordering wave vectors $\pm \mathbf{Q}_\mu$ ($\mu = 1, 2, 3$) and $\mathbf{Q}_1 + \mathbf{Q}_2 + \mathbf{Q}_3 = \mathbf{0}$, the field $\mathbf{H}$ favors the formation of skyrmion crystals because it enables an effective interaction of the form $g\mathbf{S}(\mathbf{Q}_1) \cdot \mathbf{S}(\mathbf{Q}_2) \, \mathbf{S}(\mathbf{Q}_3) \cdot \mathbf{S}(\mathbf{0})$ [42]. The condition $\mathbf{Q}_1 + \mathbf{Q}_2 + \mathbf{Q}_3 = \mathbf{0}$ explains the importance of C_3 invariant spin systems for the stabilization of triple-$\mathbf{Q}$ spin structures, such as skyrmion [32, 39] or vortex crystals [43, 44].

Indeed, skyrmion crystals arise from a superposition of three helices with ordering wave vectors $\mathbf{Q}_\mu$ [27]:

$$S_{xy}(\mathbf{r}) = \frac{I_{xy}}{C} \sum_{\mu=1}^{3} \sin[\mathbf{Q}_\mu \cdot \mathbf{r} + \theta_\mu(l)] \mathbf{e}_\mu, \quad (3)$$

$$S_z(\mathbf{r}) = \frac{1}{C} \left[I_z \sum_{\mu=1}^{3} \cos[\mathbf{Q}_\mu \cdot \mathbf{r} + \theta_\mu(l)] + S_z^0 \right], \quad (4)$$

where $I_{xy}, I_z > 0$, S_z^0 is the uniform magnetization induced by $\mathbf{H}$, $C(\mathbf{r}) = \sqrt{S_x^2 + S_y^2 + S_z^2}$ and $\mathbf{e}_\mu$ are unit vectors in the

ab plane, satisfying $\sum_{\mu=1}^{3} \mathbf{e}_\mu = 0$. The layer index l is the third component of the verctor $\mathbf{r}$. For each helix, the spin rotates in a plane parallel to $\mathbf{H}$. The angle between the rotation plane and $\mathbf{Q}_\mu$ is arbitrary because of the $U(1)$ symmetry of $\mathcal{H}$. This freedom implies that skyrmions can have arbitrary helicity γ [14] : $\gamma = 0$ for $\mathbf{e}_\mu \parallel \mathbf{Q}_\mu$ (Néel skyrmion) while $\gamma = \pi/2$ for $\mathbf{e}_\mu \perp \mathbf{Q}_\mu$ (Bloch skyrmion).

The condition $S_z = -1$ and $S_{xy} = 0$, or $\cos(\mathbf{Q}_\mu \cdot \mathbf{r} + \theta_\mu) = -1$ is fulfilled at the center of each skyrmion, implying that [45]

$$3lQ_z + \sum_{\mu=1}^{3} \theta_\mu(l) = \pi + 2n\pi, \quad (5)$$

where n is an arbitrary integer. A translation of the SC in the ab plane is obtained by shifting the phases $\theta_\mu(l)$, subjected to the constraint (5). The choice of $\theta_\mu(l)$ corresponds to the different ways of stacking the pancake skyrmions along the c-axis, where l is the layer index. For $ABAB\cdots$ stacking ($Q_z = \pi$), we can choose $\theta_\mu(l = 0) = \pi$, and $\theta_2(l = 1) = \theta_3(l = 1) = -\theta_1(l = 1)/2 = 2\pi/3$. For $ABCABC\cdots$ stacking ($Q_z = 2\pi/3$), we have $\theta_\mu(l) = \pi$ [46].

For the Hamiltonian parameters under consideration, the three ordering wave vectors are $\mathbf{Q}_1 = (Q_{ab}, 0, Q_z)$, $\mathbf{Q}_2 = (-Q_{ab}/2, \sqrt{3}Q_{ab}/2, Q_z)$, $\mathbf{Q}_3 = (-Q_{ab}/2, -\sqrt{3}Q_{ab}/2, Q_z)$. According to (5), $\theta_\mu(l)$ changes with l if $Q_z \neq 2n\pi/3$, implying the generation of higher harmonics mQ_z (m is an integer) with a resulting exchange energy cost. In other words, skyrmion crystals are more stable for $Q_z = 0$ or $Q_z = 2\pi/3$. Indeed, a single-$\mathbf{Q}$ conical state is unstable towards the generation of a second $\mathbf{Q}$-component if [39]:

$$\mathbf{Q}_1 + \mathbf{Q}_2 + \mathbf{Q}_3 = 0. \quad (6)$$

This condition is naturally fulfilled in C_6 invariant 2D lattices and it still holds for our 3D lattice if $3Q_z = 2n\pi$. In general [46], the critical value of A that renders the single-$\mathbf{Q}$ conical state unstable is:

$$A_c = J(\mathbf{Q}_1 + \mathbf{Q}_2) - J(\mathbf{Q}_3). \quad (7)$$

Given that only collinear orderings can survive for large enough A, Eq. (7) suggests that A_c should be significantly smaller than the typical value of the exchange interaction to guarantee the existence of non-collinear multi-$\mathbf{Q}$ phases. We will see below that this simple analysis is consistent with Monte Carlo simulations of $\mathcal{H}$ based on the standard Metropolis algorithm [46]. The results presented here are obtained on finite lattices of $36 \times 36 \times 36$ spins with periodic boundary conditions.

We first consider the case of NN FM interlayer exchange $J_1^c < 0$ (uniform along the c-axis) and anisotropy $A = 0.5|J_1|$. The resulting phase diagram is shown in Fig. 1 (a). Similarly to the 2D case, [32, 33, 39] a vertical spiral (VS) phase (polarization plane parallel to $\mathbf{H}$) appears in the low field and low temperature region of the phase diagram. The propagation wave vectors are $\mathbf{Q}_1 = (Q_x, 0, 0)$ and the other two vectors obtained by rotations of $\pm 120°$ about the c-axis. A triangular

crystal of vertical (parallel to $\boldsymbol{H}$) skyrmion lines is stabilized below the saturation field. The SC occupies a large region of the phase diagram because Eq. (6) is fulfilled ($mQ_z = 0$ implying no exchange energy cost due to generation of higher harmonics). Indeed, the phase diagram is quite similar to its 2D counterpart, [32, 33, 39] except for the appearance of a low-field collinear modulated (CM) phase, similar to a spin density wave, right next to the paramagnetic (PM) state [47].

We next consider a frustrated interlayer interaction ($J_1^c < 0$ and NNN inter-layer exchange $J_2^c > 0$). The resulting smooth modulation along the c-axis, $Q_z = 2\pi/5$ [$J_2^c = -J_1^c/4\cos(Q_z)$], violates the the condition (6). The low-field and low-T phase is still a VS, while a CM phase with the same ordering wave vector appears just below T_N. A pancake skyrmion crystal (PSC) is still stabilized for small J_1^c and intermediate magnetic field values. However, the size of this skyrmion phase is significantly reduced [see Figs. 1 (a) and (b)], as a consequence of the deviation from the condition (6). The skyrmion centers are still smoothly connected in neighboring layers for a small Q_z. However, as shown in Fig. 2 (b), the new c-axis modulation has the effect of tilting the skyrmion lines *away* from the field axis, leading to a tilted skyrmion line crystal (TSLC). The tilting angle α must be compatible with the period $\tilde{c} = 2\pi/Q_z$ along the vertical direction. The minimum angle α that satisfies this condition is obtained by tiling the skyrmion lines along a direction (e.g. [010]) connecting nearest-neighbor (NN) skyrmions (higher values of α are penalized by the inter-layer exchange because they increase the amplitude of higher harmonics mQ_z). Given the lattice constant of the SC in one layer is $\tilde{a} = 4\pi/\sqrt{3}Q_{ab}$, we get $\tan\alpha = \tilde{a}/\tilde{c} = 2Q_z/\sqrt{3}Q_{ab}$ for the optimal tilting angle. If the skyrmion lines are tilted in the [010] direction, a skyrmion center of the l-th layer is located at $R_0(l) = (0, l\tan\alpha)$. According to Eqs. (3) and (4), the phases $\theta_\mu(l)$ result from the condition

$$(Q_{\mu,y}\tan\alpha + Q_z)l + \theta_\mu(l) = 3Q_z l + \theta_1(l) + \theta_2(l) + \theta_3(l) = \pi, \quad (8)$$

which describes the configuration shown in Fig. 2. Upon further increasing H, the SC undergoes a transition into a double-Q conical (DQC) phase with the spins canted toward the field
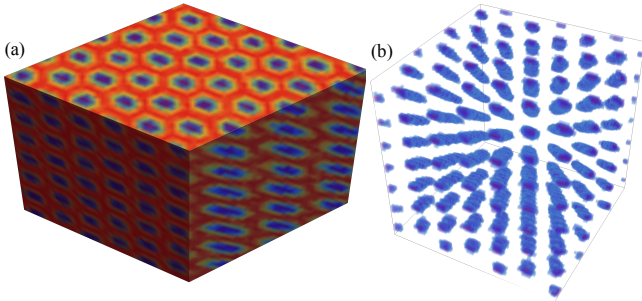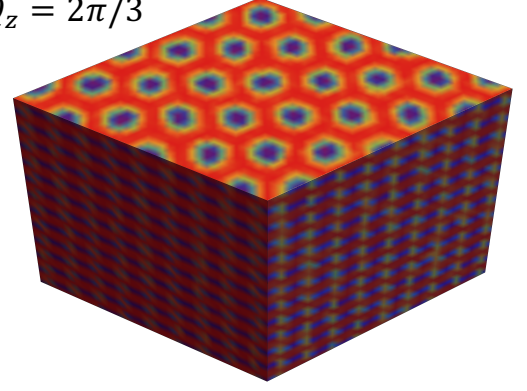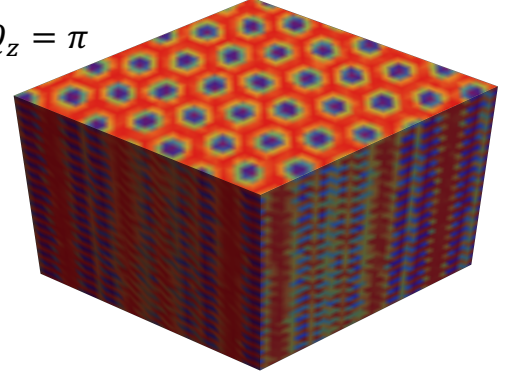

FIG. 2. (color online) (a) Skyrmion spin configuration at the surface of the simulation box for the titled skyrmion line crystal phase in Fig. 1 (b) ($Q_z = 2\pi/5$). The color represents the z spin component. (b) Arrangement of skyrmion cores (blue) defined by $S_z < -0.4$.
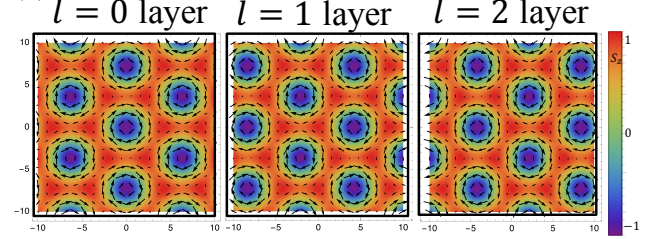
(a) $Q_z = 2\pi/3$

(b) $Q_z = \pi$

(c)

FIG. 3. (color online) Same as Fig. 2 but with (a) $Q_z = 2\pi/3$ and (b) $Q_z = \pi$. (c) Spin configuration at different layers are described by Eqs. (3), (4) and (9), where $\theta_i(l)$ is chosen to produce the FCC-PSC, corresponding to $ABCABC\cdots$ stacking with $Q_z = 2\pi/3$.

direction and the transverse components rotating with two different propagation wave vectors.

For $Q_z = 2\pi/3$ (frustrated exchange interaction along the c-axis), the projection of pancake skyrmion on the adjacent layers lies at the center of the triangle formed by NN skyrmions on those layers. This situation is energetically favored because the magnetization at the skyrmion core is opposite to the magnetization at the center of the triangle formed by three skyrmions (interstitial). The $ABCABC\cdots$ stacking (3-layer period consistent with $Q_z = 2\pi/3$) shown in Fig. 3 (a) corresponds to a face centered cubic (FCC) pancake skyrmion crystal (FCC-PSC). Given that each skyrmion center satisfies the condition $S_z(R_i) = -1$, the skyrmion position $\boldsymbol{R}_i(l) =$
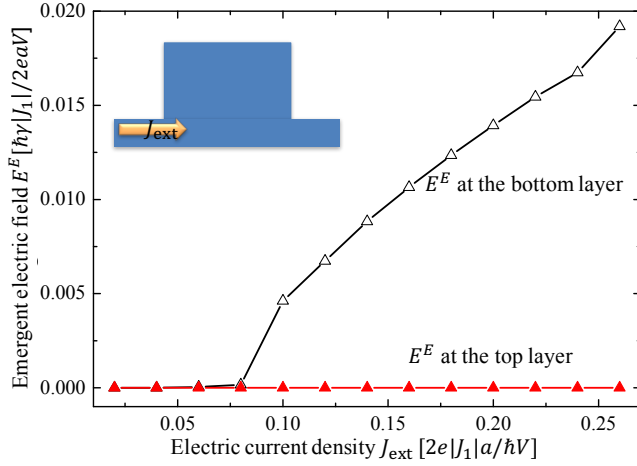
FIG. 4. (color online) Emergent longitudinal electric field as a function of current J_{ext} applied at the bottom layer. The Hamiltonian parameters are the same as in Fig. 1 (d) with $H = 0.64|J_1|$. Here a and V in the units are the lattice parameter and volume of a unit cell, respectively.

$[x(l), y(l)]$ at l-th layer is determined from

$$\boldsymbol{Q}_{\nu,ab} \cdot \boldsymbol{R}_i + Q_z l + \theta_\nu(l) = (2n_\nu + 1)\pi, \qquad (9)$$

where $\nu = 1, 2$ and n_ν are integer numbers. Here $\theta_\mu(l)$ satisfies Eq. (5). We now fix one pancake skyrmion center at $\boldsymbol{R}_0(l = 0) = (0, 0)$, i.e., $\theta_\mu(l = 0) = \pi$ for $\mu = 1, 2, 3$. For $l = 1$, a pancake skyrmion center is located at $\boldsymbol{R}_0(l = 1) = (\tilde{a}/\sqrt{3}, 0)$. The sequence shown in the three consecutive panels of Fig. 3(c) is obtained by selecting $\theta_\mu(l) = \pi$ for all layers. Figure 3 (c) shows the resulting spin configurations for the $l = 0, l = 1$ and $l = 2$ layers. As shown in Fig. 1(c) for $J_2^c = 0.5J_1^c = -0.5J_1$, the FCC-PSC occupies a wide region of the phase diagram because Eq. (6) is fulfilled.

The strongest deviation from Eq. (6) corresponds to $Q_z = \pi$. Figure 1 (d) shows the H-T phase diagram obtained for $J_1^c = -0.2J_1$ and $J_2^c = 0$. The resulting spin configuration is the $ABAB\cdots$ stacking of pancake skyrmions shown in Fig. 3 (b) corresponding to a hexagonal closed-packed (HCP) PSC. To reproduce the HCP-PSC with the ansatz of (9), we can choose the pancake skyrmion positions at layers $l = 0$ and $l = 1$ to be the same as for the FCC-PSC and repeat the pattern for even and odd layer: $\theta_\mu(l = 0) = \pi$ and $\theta_2(l = 1) = \theta_3(l = 1) = -\theta_1(l = 1)/2 = 2\pi/3$. The HCP-PSC is suppressed for large enough values of the AFM interlayer exchange [46].

A moderate easy-axis anisotropy is essential for stabilizing the above-described skyrmion crystals. However, a strong deviation from Eq. (6) will drastically reduce the stability of any multi-$\boldsymbol{Q}$ ordering [46].

The skyrmion crystals discussed so far arise from a superposition of three helices. To demonstrate the particle nature of pancake skyrmions, we inject an inhomogeneous current. The spin dynamics obeys the Landau-Lifshitz-Gilbert equation

$$\partial_t \boldsymbol{S} = \frac{\hbar\gamma}{2e}(\boldsymbol{I}_{\text{ext}} \cdot \nabla)\boldsymbol{S} - \gamma\boldsymbol{S} \times \boldsymbol{H}_{\text{eff}} + \alpha\boldsymbol{S} \times \partial_t\boldsymbol{S}, \qquad (10)$$

where γ is the gyromagnetic ratio, α is the Gilbert damping constant, $\boldsymbol{H}_{\text{eff}} \equiv -\delta\mathcal{H}/\delta\boldsymbol{S}$ is the effective magnetic field and $\boldsymbol{I}_{\text{ext}} = \boldsymbol{J}_{\text{ext}}\delta_{l,0}$ is the spin polarized current injected at the bottom layer $l = 0$. The current flows in the [100] direction of the hexagonal spin lattice. The emergent electric field induced by the skyrmion motion, $\boldsymbol{E}^E = \hbar\boldsymbol{S} \cdot (\nabla\boldsymbol{S} \times \partial_t\boldsymbol{S})/(2e)$, is proportional to the skyrmion velocity. The resulting $\boldsymbol{E}^E$ for the HCP-PSC at the bottom and top surfaces are shown in Fig. 4. Skyrmions remain pinned by the discrete spin lattice for small currents. Pancake skyrmions in the bottom layer start moving (nonzero E^E) when the current reaches a threshold value, while the skyrmions at the top surface remain at rest. We have not observed an intermediate region, where skyrmions at the top surface are dragged by the motion of skyrmion in the bottom layer. Such an intermediate region has been observed in chiral skyrmion phase [48]. The absence of the intermediate region in the HCP pancake skyrmion lattice is probably due to the fact that the skyrmion pinning force is stronger than the coupling between skyrmions in adjacent layers. The weak interlayer coupling allows pancake skyrmions to decouple from other layers. The particle nature of the pancake skyrmion can also be seen from a metastable configuration of pancake skyrmions obtained by simulated annealing [46].

In summary, we have demonstrated that different 3D skyrmion crystals can be stabilized in centro-symmetric magnets by tuning the ratio between competing inter-layer exchange interactions. Pancake skyrmions stack uniformly along the c-axis (magnetic field direction) for FM interlayer coupling ($Q_z = 0$), leading to a triangular lattice of skyrmion lines. A small Q_z has the effect of tilting the skyrmion lines away from the c-axis. Much larger values of Q_z lead to an HCP-PSC for $Q_z = \pi$ and an FCC-PSC for $Q_z = 2\pi/3$. As expected from the analysis that lead to Eq. (6), the skyrmion crystals are more stable for $Q_z = 0$ and $Q_z = 2\pi/3$. These novel spin configurations can be realized in rare-earth magnets with Ruderman-Kittel-Kasuya-Yosida interaction and moderate easy-axis anisotropy [49], as well as in frustrated magnets [50]. Finally, we note that superconducting pancake vortices of layered superconductors can also stack at a finite angle relative to the magnetic field direction because of the underlying crystal anisotropy [51]. However, HCP or FCC crystals of pancake vortices have never been observed.

* szl@lanl.gov

[1] S. Mühlbauer, B. Binz, F. Jonietz, C. Pfleiderer, A. Rosch, A. Neubauer, R. Georgii, and P. Böni, "Skyrmion lattice in a chiral magnet," Science **323**, 915 (2009).

[2] X. Z. Yu, Y. Onose, N. Kanazawa, J. H. Park, J. H. Han, Y. Matsui, N. Nagaosa, and Y. Tokura, "Real-space observation of a two-dimensional skyrmion crystal," Nature **465**, 901 (2010).

[3] K. Everschor, M. Garst, B. Binz, F. Jonietz, S. Mühlbauer, C. Pfleiderer, and A. Rosch, "Rotating skyrmion lattices by spin torques and field or temperature gradients," Phys. Rev. B **86**, 054432 (2012).

[4] J. S. White, I. Levatic, A. A. Omrani, N. Egetenmeyer, K. Prsa, I. Zivkovic, J. L. Gavilano, J. Kohlbrecher, M. Bartkowiak, H. Berger, and H. M. Ronnow, "Electric field control of the skyrmion lattice in Cu$_2$OSeO$_3$," J. Phys.: Condens. Matter **24**, 432201 (2012).

[5] Y.-H. Liu, Y.-Q. Li, and J. H. Han, "Skyrmion dynamics in multiferroic insulators," Phys. Rev. B **87**, 100402 (2013).

[6] J. S. White, K. Prša, P. Huang, A. A. Omrani, I. Živković, M. Bartkowiak, H. Berger, A. Magrez, J. L. Gavilano, G. Nagy, J. Zang, and H. M. Rønnow, "Electric-field-induced skyrmion distortion and giant lattice rotation in the magnetoelectric insulator Cu$_2$OSeO$_3$," Phys. Rev. Lett. **113**, 107203 (2014).

[7] L. Y. Kong and J. D. Zang, "Dynamics of an insulating skyrmion under a temperature gradient," Phys. Rev. Lett. **111**, 067203 (2013).

[8] S.-Z. Lin, C. D. Batista, C. Reichhardt, and A. Saxena, "ac current generation in chiral magnetic insulators and skyrmion motion induced by the spin Seebeck effect," Phys. Rev. Lett. **112**, 187203 (2014).

[9] M. Mochizuki, X. Z. Yu, S. Seki, N. Kanazawa, W. Koshibae, J. Zang, M. Mostovoy, Y. Tokura, and N. Nagaosa, "Thermally driven ratchet motion of a skyrmion microcrystal and topological magnon Hall effect," Nature Materials **13**, 241 (2014).

[10] F. Jonietz, S. Mühlbauer, C. Pfleiderer, A. Neubauer, W. Münzer, A. Bauer, T. Adams, R. Georgii, P. Böni, R. A. Duine, K. Everschor, M. Garst, and A. Rosch, "Spin transfer torques in MnSi at ultralow current densities," Science **330**, 1648 (2010).

[11] X. Z. Yu, N. Kanazawa, W. Z. Zhang, T. Nagai, T. Hara, K. Kimoto, Y. Matsui, Y. Onose, and Y. Tokura, "Skyrmion flow near room temperature in an ultralow current density," Nat. Commun. **3**, 988 (2012).

[12] T. Schulz, R. Ritz, A. Bauer, M. Halder, M. Wagner, C. Franz, C. Pfleiderer, K. Everschor, M. Garst, and A. Rosch, "Emergent electrodynamics of skyrmions in a chiral magnet," Nat. Phys. **8**, 301 (2012).

[13] A. Fert, V. Cros, and J. Sampaio, "Skyrmions on the track," Nat. Nanotechnol. **8**, 152–156 (2013).

[14] N. Nagaosa and Y. Tokura, "Topological properties and dynamics of magnetic skyrmions," Nature Nanotechnology **8**, 899–911 (2013).

[15] W.J. Jiang, G. Chen, K. Liu, J. D. Zang, S. G. E. te Velthuis, and A. Hoffmann, "Skyrmions in magnetic multilayers," Phys. Rep. **704**, 1–49 (2017).

[16] A. Fert, N. Reyren, and V. Cros, "Magnetic skyrmions: advances in physics and potential applications," Nature Reviews Materials **2**, 17031 (2017).

[17] X. Z. Yu, N. Kanazawa, Y. Onose, K. Kimoto, W. Z. Zhang, S. Ishiwata, Y. Matsui, and Y. Tokura, "Near room-temperature formation of a skyrmion crystal in thin-films of the helimagnet FeGe," Nat. Mater **10**, 106 (2011).

[18] T. Adams, A. Chacon, M. Wagner, A. Bauer, G. Brandl, B. Pedersen, H. Berger, P. Lemmens, and C. Pfleiderer, "Long-wavelength helimagnetic order and skyrmion lattice phase in Cu$_2$OSeO$_3$," Phys. Rev. Lett. **108**, 237204 (2012).

[19] S. Seki, X. Z. Yu, S. Ishiwata, and Y. Tokura, "Observation of skyrmions in a multiferroic material," Science **336**, 198 (2012).

[20] I. Dzyaloshinsky, "A thermodynamic theory of weak ferromagnetism of antiferromagnetics," J. Phys. Chem. Solids **4**, 241 (1958).

[21] T. Moriya, "Anisotropic superexchange interaction and weak ferromagnetism," Phys. Rev. **120**, 91 (1960).

[22] T. Moriya, "New mechanism of anisotropic superexchange interaction," Phys. Rev. Lett. **4**, 228–230 (1960).

[23] A. N. Bogdanov and D. A. Yablonskii, "Thermodynamically stable "vortices" in magnetically ordered crystals: The mixed state of magnets," Sov. Phys. JETP **68**, 101 (1989).

[24] A. Bogdanov and A. Hubert, "Thermodynamically stable magnetic vortex states in magnetic crystals," J. Magn. Magn. Mater. **138**, 255 – 269 (1994).

[25] U. K. Rößler, A. N. Bogdanov, and C. Pfleiderer, "Spontaneous skyrmion ground states in magnetic metals," Nature **442**, 797 (2006).

[26] G. H. Derrick, "Comments on nonlinear wave equations as models for elementary particles," J. Math. Phys. **5**, 1252 (1964).

[27] T. Okubo, S. Chung, and H. Kawamura, "Multiple-q states and the skyrmion lattice of the triangular-lattice heisenberg antiferromagnet under magnetic fields," Phys. Rev. Lett. **108**, 017206 (2012).

[28] X. Z. Yu, M. Mostovoy, Y. Tokunaga, W. Z. Zhang, K. Kimoto, Y. Matsui, Y. Kaneko, N. Nagaosa, and Y. Tokura, "Magnetic stripes and skyrmions with helicity reversals," PNAS **109**, 8856–8860 (2012).

[29] D. Solenov, D. Mozyrsky, and I. Martin, "Chirality waves in two-dimensional magnets," Phys. Rev. Lett. **108**, 096403 (2012).

[30] R. Ozawa, S. Hayami, K. Barros, G.-W. Chern, Y. Motome, and C. D. Batista, "Vortex Crystals with Chiral Stripes in Itinerant Magnets," J. Phys. Soc. Jpn. **85**, 103703 (2016).

[31] D. Wulferding, H. Kim, I. Yang, J. Jeong, K. Barros, Y. Kato, I. Martin, O. E. Ayala-Valenzuela, M. Lee, H. C. Choi, F. Ronning, L. Civale, R. E. Baumbach, E. D. Bauer, J. D. Thompson, R. Movshovich, and Jeehoon Kim, "Domain engineering of the metastable domains in the 4f-uniaxial-ferromagnet CeRu$_2$Ga$_2$B," Scientific Reports **7**, 46296 (2017).

[32] A. O. Leonov and M. Mostovoy, "Multiply periodic states and isolated skyrmions in an anisotropic frustrated magnet," Nature Communications **6**, 8275 (2015).

[33] S.-Z. Lin and S. Hayami, "Ginzburg-Landau theory for skyrmions in inversion-symmetric magnets with competing interactions," Phys. Rev. B **93**, 064430 (2016).

[34] L. Rózsa, A. Deák, E. Simon, R. Yanes, L. Udvardi, L. Szunyogh, and U. Nowak, "Skyrmions with attractive interactions in an ultrathin magnetic film," Phys. Rev. Lett. **117**, 157205 (2016).

[35] P. Sutcliffe, "Skyrmion knots in frustrated magnets," Phys. Rev. Lett. **118**, 247203 (2017).

[36] R. Ozawa, S. Hayami, and Y. Motome, "Zero-field skyrmions with a high topological number in itinerant magnets," Phys. Rev. Lett. **118**, 147205 (2017).

[37] Y. A. Kharkov, O. P. Sushkov, and M. Mostovoy, "Bound states of skyrmions and merons near the lifshitz point," Phys. Rev. Lett. **119**, 207201 (2017).

[38] X. C. Zhang, J. Xia, Y. Zhou, X. X. Liu, H. Zhang, and M. Ezawa, "Skyrmion dynamics in a frustrated ferromagnetic film and current-induced helicity locking-unlocking transition," Nature Communications **8**, 1717 (2017).

[39] S. Hayami, S.-Z. Lin, and C. D. Batista, "Bubble and skyrmion

crystals in frustrated magnets with easy-axis anisotropy," Phys. Rev. B **93**, 184413 (2016).

[40] W. H. Wang, Y. Zhang, G. Z. Xu, L. C. Peng, B. Ding, Y. Wang, Z. P. Hou, X. M. Zhang, X. Y. Li, E. K. Liu, S. G. Wang, J. W. Cai, F. W. Wang, J. Q. Li, F. X. Hu, G. H. Wu, B. G. Shen, and X.-X. Zhang, "A Centrosymmetric Hexagonal Magnet with Superstable Biskyrmion Magnetic Nanodomains in a Wide Temperature Range of 100-340 K," Adv. Mater. **28**, 6887–6893 (2016).

[41] The in-plane wave vector components are in units of a^{-1}, where a is the triangular lattice parameter, while the out of plane component, Q_z, is in units of c^{-1}, where c is the lattice parameter along the direction perpendicular to the triangular layers.

[42] T. Garel and S. Doniach, "Phase transitions with spontaneous modulation-the dipolar Ising ferromagnet," Phys. Rev. B **26**, 325–329 (1982).

[43] Y. Kamiya and C. D. Batista, "Magnetic vortex crystals in frustrated Mott insulator," Phys. Rev. X **4**, 011023 (2014).

[44] Z. T. Wang, Y. Kamiya, A. H. Nevidomskyy, and C. D. Batista, "Three-dimensional crystallization of vortex strings in frustrated quantum magnets," Phys. Rev. Lett. **115**, 107201 (2015).

[45] O. Petrova and O. Tchernyshyov, "Spin waves in a skyrmion crystal," Phys. Rev. B **84**, 214433 (2011).

[46] See Supplemental Material, which includes Refs. [32, 33, 39, 52].

[47] This phase also appears in a mean field treatment of the problem.

[48] S.-Z. Lin and A. Saxena, "Dynamics of Dirac strings and monopolelike excitations in chiral magnets under a current drive," Phys. Rev. B **93**, 060401 (2016).

[49] J. Jensen and A. R. Mackintosh, *Rare Earth Magnetism: Structures and Excitations* (Clarendon Press, Oxford, 1991).

[50] C. D. Batista, S.-Z. Lin, S. Hayami, and Y. Kamiya, "Frustration and chiral orderings in correlated electron systems," Rep. Prog. Phys **79**, 084504 (2016).

[51] G. Blatter, M. V. Feigel'man, V. B. Geshkenbein, A. I. Larkin, and V. M. Vinokur, "Vortices in high-temperature superconductors," Rev. Mod. Phys. **66**, 1125–1388 (1994).

[52] C. Serpico, I. D. Mayergoyz, and G. Bertotti, "Numerical technique for integration of the Landau-Lifshitz equation," J. Appl. Phys. **89**, 6991–6993 (2001).